JOC Article

Reaction of Diphenyldiazomethane with Singlet Oxygen Studied by Time-Resolved IR Spectroscopy

Joel Torres-Alacan and Wolfram Sander*

Lehrstuhl für Organische Chemie II der Ruhr-Universität, D-44780 Bochum, Germany

wolfram.sander@rub.de

Received May 2, 2008

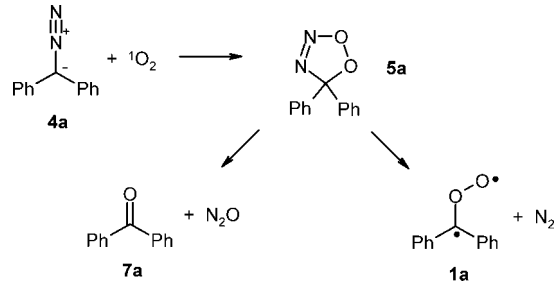

The mechanism of the reaction of diphenyldiazomethane **4a** with singlet oxygen has been investigated by nanosecond time-resolved UV−vis (LFP) and IR (step-scan) spectroscopy. The experiments were performed with fullerene (C_{60}) as photosensitizer for the generation of $^1O_2$ in nonpolar solvents (toluene and CCl_4). The UV−vis experiments allowed us to monitor the formation of benzophenone *O*-oxide **1a**, while in the IR experiments the bleaching of **4a** and the formation of benzophenone **7a** and N_2O was observed. The kinetic data were evaluated using Monte Carlo simulation and DFT calculations. These methods allow us to present a consistent mechanistic scheme for the reaction of **4a** with $^1O_2$ and to explain why the elusive dioxadiazole **5a** as key intermediate is not directly observed.

Introduction

Carbonyl oxides **1** are highly reactive, powerful oxidants that are far less investigated than their isomeric dioxiranes **2**.[1−3] The rearrangement to dioxiranes requires photochemical activation and has been used for the synthesis of stable dioxiranes.[4] The thermal cyclization of **1** to **2** has never been observed.

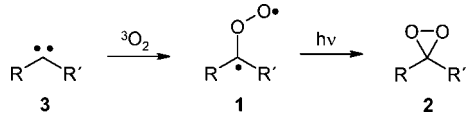

There are several routes for the synthesis of carbonyl oxides **1**: (i) the cycloreversion of 1,2,3-trioxolanes during the ozonolysis of alkenes (Criegee reaction);[5−7] (ii) the reaction of triplet carbenes **3** with molecular (triplet) oxygen, the triplet route;[8,9] and (iii) the reaction of diazo compounds **4** with singlet oxygen,

SCHEME 1. Mechanism of the Synthesis of Carbonyl Oxides 1 via the Singlet Route from Diazo Compounds 4

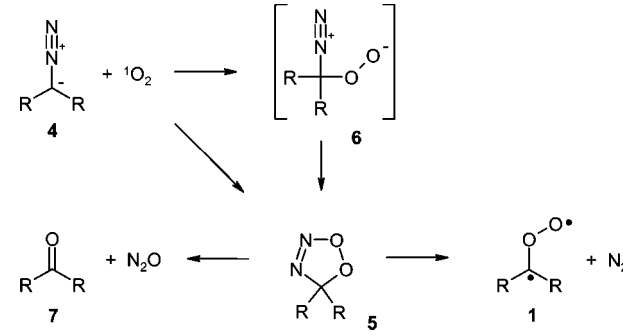

(1) Sander, W. W.; Patyk, A.; Bucher, G. *J. Mol. Struct.* **1990**, *222*, 21–31.
(2) Block, K.; Kappert, W.; Kirschfeld, A.; Muthusamy, S.; Schroeder, K.; Sander, W.; Kraka, E.; Sosa, C.; Cremer, D. *Peroxide Chem.* **2000**, 139–156.
(3) Sander, W.; Block, K.; Kappert, W.; Kirschfeld, A.; Muthusamy, S.; Schroeder, K.; Sosa, C. P.; Kraka, E.; Cremer, D. *J. Am. Chem. Soc.* **2001**, *123*, 2618–2627.
(4) Sander, W.; Schroeder, K.; Muthusamy, S.; Kirschfeld, A.; Kappert, W.; Boese, R.; Kraka, E.; Sosa, C.; Cremer, D. *J. Am. Chem. Soc.* **1997**, *119*, 7265–7270.
(5) Criegee, R.; Wenner, G. *Liebigs Ann. Chem.* **1949**, *564*, 9–15.
(6) Criegee, R. *Angew. Chem.* **1975**, *87*, 765–771.
(7) Story, P. R.; Burgess, J. R. *J. Am. Chem. Soc.* **1967**, *89*, 5726–5727.
(8) Bartlett, P. D.; Traylor, T. G. *J. Am. Chem. Soc.* **1962**, *84*, 3408–3409.
(9) Casal, H. L.; Tanner, M.; Werstiuk, N. H.; Scaiano, J. C. *J. Am. Chem. Soc.* **1985**, *107*, 4616–4620.

10.1021/jo800955w CCC: $40.75
Published on Web 08/14/2008

the singlet route.[9−13] While there has been a lot of indirect evidence collected that carbonyl oxides **1** are indeed intermediates in the Criegee reaction, so far it was not possible to detect **1** as an intermediate in these reactions by direct spectroscopic methods. If **1** is indeed formed (which is generally accepted), it is too short-lived to be directly detected under these conditions. In contrast, the reaction of carbenes with $^3O_2$ is very efficient and makes it possible to detect **1** via laser flash photolysis (LFP) in solution[9] or via matrix isolation spectroscopy at cryogenic temperatures in inert matrices.[14−17] As expected, triplet carbenes react much faster than singlet carbenes; however, in low temperature matrices it was also possible to obtain carbonyl oxides by oxygenation of singlet carbenes such as phenylchlorocarbene.[18] By reacting the sterically hindered dimesitylcarbene with $^3O_2$, a kinetically stabilized carbonyl oxide was synthesized that at −78 °C was stable enough to be characterized via NMR spectroscopy.[19] The disadvantage of the triplet route is the intermediacy of highly reactive carbenes **3**, which frequently results in unwanted side reactions.

The singlet route also starts from diazo compounds **4** but circumvents the formation of free carbenes **3**. The key intermediate of the singlet route is 1,2,3,4-dioxadiazole **5**, a short-lived heterocycle that decays via fast cycloreversions either to a carbonyl oxide **1** and N_2 or to a ketone **7** and N_2O (Scheme 1). The dioxadiazole **5** is formed either via a concerted 1,3-dipolar cycloaddition of **4** and $^1O_2$[20] or stepwise with zwitterion **6** as an intermediate. Neither **5** nor **6** has been observed by direct spectroscopic methods so far, and all experimental evidence comes from measuring the ratio of N_2O/N_2 by gas chromatography by Sawaki et al.[11,21]

Benzophenone *O*-oxide **1a** (R = Ph) is the prototype of a carbonyl oxide and was investigated by classical trapping, matrix isolation,[16] and UV−vis nanosecond time-resolved spectroscopy (LFP).[13] In solution **1a** was produced via both the triplet and the singlet route as a relatively long-lived intermediate (>100 μs) with an absorption maximum at 410 nm.[13] As a result of the strong visible absorption at $\lambda = 410$ nm, carbonyl oxide **1a** is readily detected in LFP experiments, while the other proposed intermediates or products (Scheme 1) are not observable under these conditions. Here, we describe a combined time-resolved UV−vis and IR investigation of the reaction of diphenyldiazomethane **4a** with $^1O_2$. The combination of time-resolved IR spectroscopy with a time resolution of about 100 ns and UV−vis spectroscopy with 10 ns time resolution provides detailed insight into the singlet route for the synthesis of carbonyl oxides **1**.

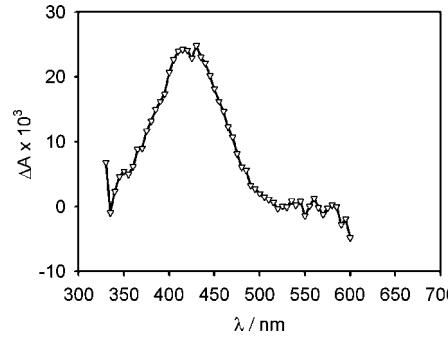

FIGURE 1. Transient spectrum recorded 11 μs after the 532 nm excitation (6−7 ns, ~130 mJ/pulse) of a solution of C_{60} (0.0132 mmol/L), **4a** (1 mmol/L), and O_2 (9.88 mmol/L) in toluene. The triangles represent experimental points. Averaging over a 1 μs time window (10 data points) was performed to improve the signal-to-noise ratio. The peak at 410 nm is assigned to carbonyl oxide **1a**.

Results and Discussion

LFP with UV−vis Detection. In the LFP experiments reported by Scaiano et al., acetonitrile was used as solvent and methylene blue with 587-nm excitation as triplet sensitizer for the generation of $^1O_2$.[13] Since in our experiments shorter wavelength excitation at 532 nm (second harmonic of a Nd:YAG laser) was used where methylene blue has a very low absorption coefficient, we used fullerene (C_{60}) as sensitizer. In toluene the absorption maxima of fullerene are at 457, 509, and 747 nm,[22] and the lifetime of its triplet state is estimated to >0.28 ms.[22] Since the quantum yield of phosphorescence is very low, the main mechanism of deactivation presumably is triplet-triplet annihilation. Fullerene as sensitizer has the additional advantages that in nonpolar solvents such as toluene or CCl_4 it is much more soluble than methylene blue and that it is photochemically more stable.

Several blind experiments proved that C_{60} is indeed an efficient sensitizer for the formation of $^1O_2$ and that diphenyldiazomethane **4a** is only bleached in the presence of both C_{60} and molecular oxygen. Thus, after excitation (532-nm laser pulse) of a 1 mmol/L solution of **4a** in toluene in the absence of C_{60}, no reaction or transient is observed in the absence or presence of dissolved oxygen. Irradiation of an argon-purged solution of C_{60} produces the expected long-lived triplet C_{60}, which in the presence of oxygen is rapidly quenched (see Supporting Information, Figure S4).

If a solution of **4a** and C_{60} in toluene is excited in the absence of oxygen, only the transient $^3C_{60}$ is observed. In the presence of oxygen and otherwise identical conditions, however, the strong 410-nm absorption of **1a** is easily detected. The UV−vis absorption spectrum of **1a** (Figure 1) formed under these conditions is in excellent agreement with the data reported by Scaiano et al.,[13] which clearly show that C_{60} is a suitable sensitizer for the generation of $^1O_2$ in LFP experiments. For the formation of **1a**, a pseudo-first-order rate constant of $(2.2 \pm 0.3) \times 10^5$ s^{-1} is found (Table 1, Figure 2). The decay of **1a** is a second-order process (dimerization)[13] and clearly much slower than its formation. The formation of **1a** and the bleaching of **4a** (see below) corresponds to rise and decay times on the order of 2 μs, which is clearly much shorter than the lifetime

(10) Higley, D. P.; Murray, R. W. *J. Am. Chem. Soc.* **1976**, *98*, 4526–4533.
(11) Nojima, T.; Ishiguro, K.; Sawaki, Y. *Chem. Lett.* **1995**, 545–546.
(12) Casal, H. L.; Sugamori, S. E.; Scaiano, J. C. *J. Am. Chem. Soc.* **1984**, *106*, 7623–7624.
(13) Scaiano, J. C.; McGimpsey, W. G.; Casal, H. L. *J. Org. Chem.* **1989**, *54*, 1612–1616.
(14) Bell, G. A.; Dunkin, I. R. *J. Chem. Soc., Chem. Commun.* **1983**, 1213–1215.
(15) Dunkin, I. R.; Bell, G. A. *Tetrahedron* **1985**, *41*, 339–347.
(16) Sander, W. *Angew. Chem.* **1986**, *98*, 255–256.
(17) Bucher, G.; Sander, W. *Chem. Ber.* **1992**, *125*, 1851–1859.
(18) Ganzer, I.; Hartmann, M.; Frenking, G. *Chem. Org,c Germanium, Tin Lead Compd.* **2002**, *2*, 169–282.
(19) Sander, W.; Marquardt, R.; Bucher, G.; Wandel, H. *Pure Appl. Chem.* **1996**, *68*, 353–356.
(20) Bethell, D.; McKeivor, R. *J. Chem. Soc., Perkin Trans.* **1977**, *2*, 327–333.
(21) Nojima, T.; Ishiguro, K.; Sawaki, Y. *J. Org. Chem.* **1997**, *62*, 6911–6917.
(22) Ebbesen, T. W.; Tanigaki, K.; Kuroshima, S. *Chem. Phys. Lett.* **1991**, *181*, 501–504.

TABLE 1. Summary of Experimental Conditions and Kinetic Data[a]

4a (mmol/L)	C_{60} (mM, mmol/L)	$^3O_2$ (mmol/L)	solvent	rate constants (s^{-1})	experiment
~1	0.0132	9.88	toluene	$k_{growth(\mathbf{1a})} = (2.2 \pm 0.3) \times 10^5$	TR-UV−vis
~2	0.26	9.88	toluene	$k_{decay(\mathbf{4a})} = (3.32 \pm 0.09) \times 10^5$ $k_{growth(\mathbf{N2O})} = (2.8 \pm 0.4) \times 10^5$	step-scan TR-FTIR
~2.5	0.26	12.44	CCl_4	$k_{decay(\mathbf{4a})} = (5.1 \pm 0.4) \times 10^5$ $k_{growth(\mathbf{N_2O})} = (4.2 \pm 0.3) \times 10^5$ $k_{growth(\mathbf{7a})} = (4.3 \pm 0.3) \times 10^{5a}$ $k_{growth(\mathbf{7a})} = (7.2 \pm 0.4) \times 10^{5b}$	step-scan TR-FTIR

[a] Rate constant determined at 1665 cm^{-1}. [b] Rate constant determined at 1278 cm^{-1}. [a] First-order or pseudo-first-order behavior assumed. The statistical errors are shown with the kinetic data. In addition, there are systematic errors caused by uncertainties in the initial concentrations and different experimental set ups in LFP and step scan experiments.

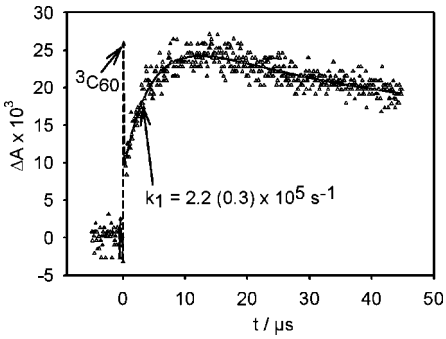

FIGURE 2. Transient trace recorded at 410 nm following 532 nm excitation (6−7 ns, ~130 mJ/pulse) of a solution of C_{60} (13.2 μmol/L), **4a** (1 mmol/L), and O_2 (9.88 mmol/L) in toluene. Experimental data were fit using a biexponential model. Exponetial rates k_1 and k_2 are indicated with standard errors in parenthesis. The dashed line indicates the residue due to $^3C_{60}$.

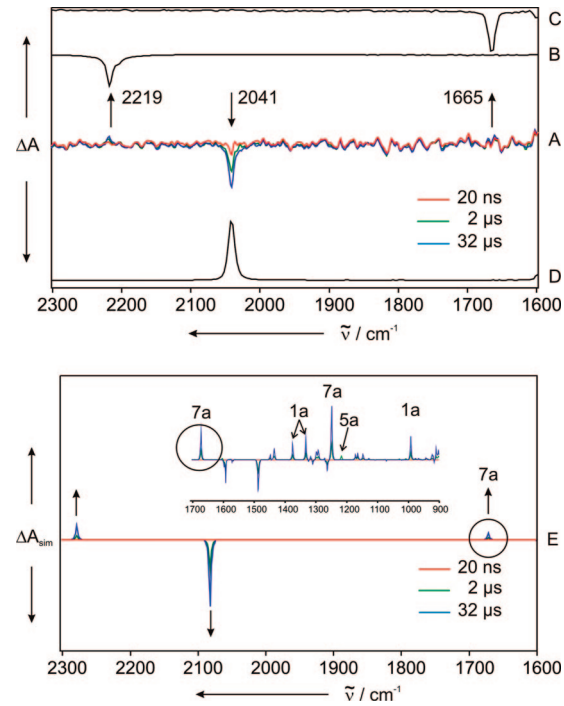

FIGURE 3. (A) Difference spectra recorded 20 ns (red), 2 μs (green), and 32 μs (blue) after 532-nm excitation (6−7 ns, ~26 mJ/pulse) of a solution of **4a** (2.5 mmol/L), C_{60} (0.26 mmol/L), and O_2 (12.44 mmol/L) in CCl_4. Besides statistical errors (noise) the spectra also show artifacts presumably caused by fluctuations of the laser intensity and a decrease of the optical quality of the sample/mirror set up during the experiments. (B) IR spectrum of N_2O in CCl_4. (C) IR spectrum of **7a** in CCl_4. (D) IR spectrum of **4a** in CCl_4. (E) Simulated difference spectra based on Monte Carlo and B3LYP/6-31G(d) calculations. Arrows indicate time evolution.

of $^1O_2$ in toluene (29 μs) or CCl_4 (700 μs).[23] Thus, the decay of $^1O_2$ in these solvents does not influence our mechanistic scheme.

Step-Scan FTIR Detection. IR experiments were performed in toluene as solvent under similar conditions as the UV−vis experiments described above, only the concentration of **4a** was increased to 2 mmol/L to optimize the IR detection (Table 1). Again, **4a** proved to be stable in the absence of oxygen and/or C_{60}. In the presence of both oxygen and C_{60}, singlet oxygen is produced and **4a** is bleached (monitored at the N≡N stretching vibration at 2041 cm^{-1}) with a pseudo-first-order rate constant of $(3.32 \pm 0.09) \times 10^5$ s^{-1}. Because of strong absorptions of toluene in large parts of the IR spectrum, N_2O with absorption at 2219 cm^{-1} was the only product observed. The rate for the formation of N_2O ($(2.8 \pm 0.4) \times 10^5$ s^{-1}) is similar to that of the decay of **4a** and the formation of **1a**.

Additional experiments were performed in CCl_4 as solvent, which has the advantage of a much higher IR transmittance in most parts of the spectrum but the disadvantage of a low solubility of C_{60}. However, since the initial experiments in toluene proved that a concentration of 0.2 mg/mL of C_{60} is high enough for the sensitization, CCl_4 is well-suited for these experiments. In CCl_4 a barely visible absorption at 1665 cm^{-1} is assigned to the C=O stretching vibration of benzophenone **7a** (Figure 3). A careful analysis of the kinetic traces at 1665 cm^{-1} clearly indicates an absorption band and not an artifact at this position. Artifacts in the difference spectra result in a background that is apparently statistic in frequency but not in time (background at different times runs parallel). Presumably, these artifacts are caused by fluctuations of the laser intensity and a decrease of the optical quality of the sample/mirror set up during the experiments. In addition, the 2219 cm^{-1} absorption of N_2O is also observed. Within the error limits the formation of **7a** and N_2O shows the same kinetics as the decay of **4a** (Figure 4). Other transients and especially any band that could be attributed to dioxadiazole **5a** or triplet **4a** could not be detected.

Kinetic Simulation. The UV−vis and IR experiments clearly show two major reaction channels of the elusive intermediate **5a**, the formation of **1a** observed in the UV−vis experiment and N_2 (not directly observed) on one hand, and the formation of **7a** and N_2O, both observed in the IR experiments, on the other hand. Although **1a** and **7a**/N_2O could not be observed in the same experiment, it is clear that both are formed simultaneously, as was deduced previously by measuring the N_2/N_2O ratio by gas chromatography.[11,21]

(23) Salokhiddinov, K. I.; Byteva, I. M.; Gurinovich, G. P. *Zh. Prikl. Spektrosk.* **1981**, *34*, 892–897.

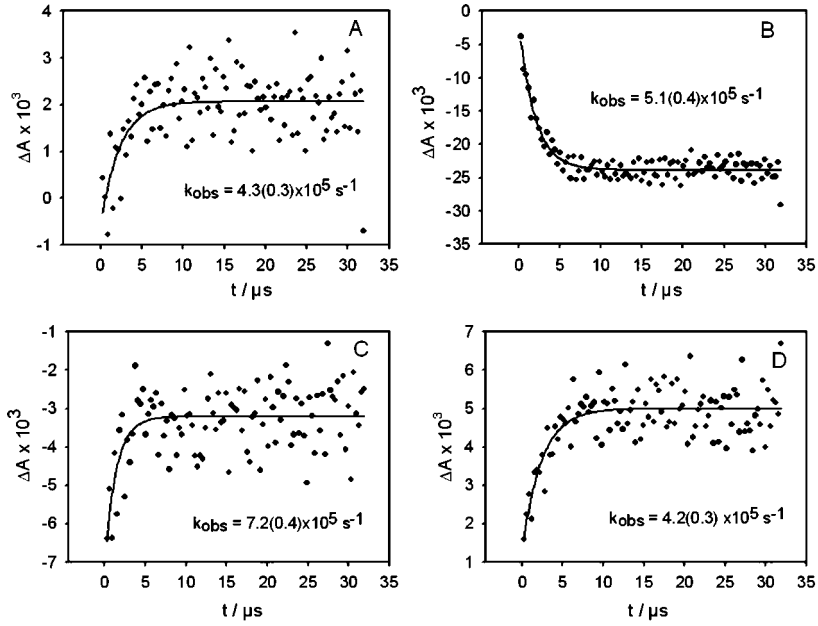

FIGURE 4. Transient traces after 532-nm excitation (6−7 ns, ∼26 mJ/pulse) monitored at (A) 1665, (B) 2041, (C) 1278, and (D) 2219 cm^{-1}. (A) and (C) show traces assigned to **7a**, (B) is assigned to **4a**, and (D) is assigned to N_2O. Solid curves show least-squares fits to a single exponential.

SCHEME 2. Mechanistic Scheme Describing the Reaction of 4a with $^1O_2$

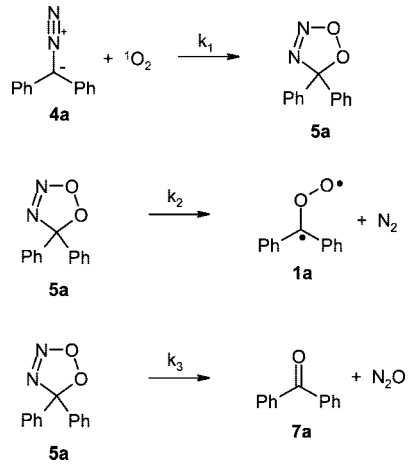

To describe the formation of **1a** and **7a** from **4a** and singlet oxygen, a simple mechanistic scheme with **5a** as the presumed key intermediate, k_1 describing the formation of **5a**, and k_2 and k_3 describing the exit channels is used (Scheme 2). The experimental kinetic data from the LFP and step scan FTIR experiments assuming exponential decay and growth (first-order or pseudo-first-order behavior assumed) are summarized in Table 1.

The experimental kinetic data from the LFP experiments were evaluated using Monte Carlo simulation. With the three rate constants $k_1 = 7.7 \times 10^7$ L mol^{-1} s^{-1}, $k_2 = 7.81 \times 10^5$ s^{-1}, $k_3 = 5.73 \times 10^5$ s^{-1} obtained from the Monte Carlo simulation, the decay and growth of reactant and products are nicely fitted (Figure 5). The rate constant k_1 is on the order of the value obtained by quenching experiments in acetonitrile/dichloromethane by Scaiano et al. (3.6×10^8 L mol^{-1} s^{-1}). Since the formation of **5a** is the rate-limiting step (k_1), the two subsequent faster parallel reactions leading to **1a** (k_2) and **7a** (k_3), respectively, cannot be accurately determined by modeling our experimental data. Therefore, the ratio k_2/k_3 was fixed to 1.36 during the Monte Carlo simulation to be consistent with the experimental results.[21]

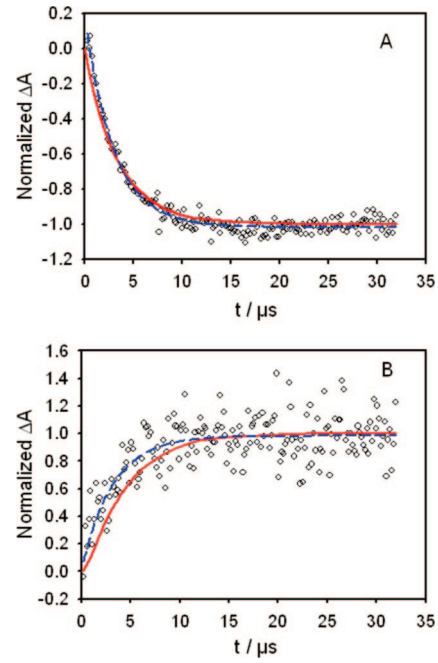

FIGURE 5. Time profile at (A) 2041 and (B) 2219 cm^{-1} after 532 nm excitation of a toluene solution containing 2 mmol/L of **4a** and 0.26 mmol/L of C_{60} saturated with $^3O_2$ (circles). In order to find the normalizing factor for the experimental data, the last 16 experimental data points were averaged. The dashed line (in blue) represents the least-squares-fit to an exponential decay function with nonzero intercept. The solid line (in red) represents the Monte Carlo simulation of **4a** based on the mechanistic scheme shown in Scheme 1. Parameters for the MC simulation: $n_1 = 280$, $n_2 = 1023$, $n_3 = 750$. A 300 × 300 grid was initialized randomly with **4a** and $^1O_2$ in a ratio of 9:1 and 2200 cycles were scaled to 32 μs ($\beta = 6.875 \times 10^7$ cycles/s). The elementary reactions were processed statistically, and four runs were averaged in order to cancel out fluctuations.

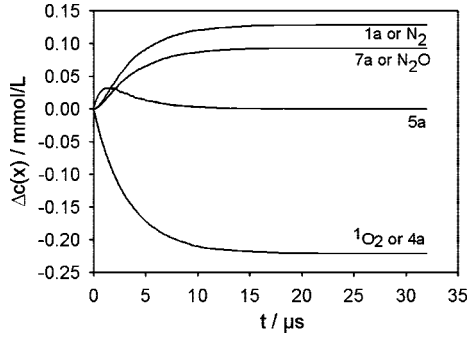

FIGURE 6. Monte Carlo simulation according to the mechanism presented in Scheme 1. Parameters for the simulation: $n_1 = 280$, $n_2 = 1023$, $n_3 = 750$, concentration scale coefficient $\alpha = 360$ L mol^{-1}. The coefficient for scaling the time was set to $\beta = 6.875 \times 10^7$ cycles s^{-1}. The elementary reactions were processed statistically, and 4 runs were averaged in order to cancel out fluctuations.

Within the detection limits of our time-resolved IR experiments, neither dioxadiazole **5a** nor carbonyl oxide **1a** could be detected. We therefore calculated the IR frequencies and absolute intensities of all species expected from our kinetic scheme using DFT calculations. The kinetic data from the Monte Carlo simulations were used to simulate the IR spectra of the product mixture at various times after the initial laser pulse (Figure 3). A comparison of the experimental difference spectra measured in CCl_4 after 20 ns, 2 μs, and 32 μs (Figure 3) with the simulation based on the DFT calculation and Monte Carlo simulation (Figure 3) reveals a very satisfying agreement.

For the simulations we assume that $^1O_2$ reacts chemically with **4a** and physical quenching producing ^{3}**4a** does not take place. Although we can not rigorously exclude physical quenching, the formation of N_2O and the bleaching of **4a** in the experiment nicely parallels that expected from the simulation. This excludes that a long-lived triplet state of **4a** is efficiently formed, since this would result in a higher ratio of bleaching of **4a** compared to the formation of N_2O. Even if physical quenching of $^1O_2$ occurs to a small extend, this would only influence the yield of the products but not the pseudo-first-order rate constants.

In the experiment the intensity of the C=O stretching vibration is about twice that of the baseline noise. Thus, bands with a lower intensity will be below the detection limit. This is indeed the case for all IR bands of **1a** and **5a**, and therefore these compounds cannot be detected in the IR experiments. The Monte Carlo integration predicts the highest concentration of **5a** to build up after 1.2 μs (Figure 6). This corresponds to an estimated concentration of 32 μmol/L, which is approximately seven times less than the detection limit.

Conclusion

Carbonyl oxides **1** are highly potent oxidants that, however, due to the lack of efficient syntheses, have not found many synthetic applications so far. The singlet route is a promising way starting from readily accessible precursors and avoiding unwanted side reactions of highly reactive carbenes. Using nanosecond time-resolved UV−vis and IR techniques in combination with Monte Carlo simulation and DFT calculations allowed us to gain mechanistic details for the synthesis of benzopheneone *O*-oxide **1a** via the singlet route. The rate-determining step of the reaction sequence is the formation of the elusive dioxadiazole **5a**. This heterocycle is highly labile and rapidly decomposes via two parallel reactions to form either the desired **1a** and N_2 or benzophenone **7a** and N_2O. The kinetic simulations reveal that the maximum concentration of **5a** building up is too low to be detectable in our experiments. The kinetic data extracted from the LFP experiments are in good agreement with the previously published scheme based on the analysis of the N_2/N_2O ratio.[21]

Experimental Section

General Methods. C_{60} (99.9%) was obtained from a commercial supplier and used without further purification; **4a** was prepared according to literature procedures.[24]

Step-Scan Time-Resolved FTIR. A modified Bruker IFS 66v/S FTIR spectrometer with step-scan option, a Nd:YAG laser, and a sample cell connected to a continuous flow system was used for the step-scan experiments. The flow cell was positioned outside the spectrometer and the IR spectra measured in reflection using a mirror unit in the spectrometer and a gold-coated mirror on the back of the flow cell. A photovoltaic MCT detector (risetime 25 ns) with internal preamplifier was used. The AC-coupled output of the preamplifier is fed directly into a second amplifier and then read out by a 200 MHz, 8 bit transient recorder connected to a PC. Positioning of the interferometer mirror and data acquisition was performed using OPUS software. The solution was pumped trough the sample cell (two CaF_2 windows, 0.4 mm Teflon spacer) by a peristaltic pump with low pulsation (Ismatec IPC-N-4, ca. 2 mL/min flow) and transferred back into a storage tank. The sample was excited using the second harmonic (532 nm) of the Nd:YAG laser with a repetition rate of 10 Hz. To avoid thermal effects and shockwaves the laser energy was attenuated to 10−18 mJ/pulse by an external attenuator. The laser beam was split by a variable dielectric attenuator, and both beams crossed the sample overlapping the IR profile (see Supporting Information for details). This reduced the laser energy density in the sample and improved the signal-to-noise ratio. During the measurements the spectrometer was evacuated to 2 mbar pressure. In order to eliminate external vibrations, the whole system was placed on a vibrationally insulated table. All measurements were carried out with 6 cm^{-1} resolution in a spectral range between 0 and 3160 cm^{-1}, resulting in an interferogram containing 1060 points. The signal was averaged 20 times per sampling position. In all experiments a time range of 32 μs was recorded with a resolution of 20 ns. After Fourier transformation the average of 20 successive spectra was calculated to achieve a better signal-to-noise ratio, resulting in an effective time resolution of 400 ns. The samples were dissolved (0.26 mmol/L C_{60}, ~2 mmol/L **4a**) in toluene and carbon tetrachloride (spectroscopic grade) and purged with argon or oxygen, respectively, for 60 min.

Nanosecond Laser Flash Photolysis. A standard LFP setup was used, consisting of a Nd:YAG laser, operated at 1 Hz and 532 nm (100 mJ/pulse, 6−7 ns pulse duration), a pulse Xe arc lamp, a

(24) Smith, L. I.; Howard, K. L. *Org. Synth.* **1944**, *24*, 53–55.
(25) Frisch, M. J.; Trucks, G. W.; Schlegel, H. B.; Scuseria, G. E.; Robb, M. A.; Cheeseman, J. R.; Montgomery, J. A., Jr.; Vreven, T.; Kudin, K. N.; Burant, J. C.; Millam, J. M.; Iyengar, S. S.; Tomasi, J.; Barone, V.; Mennucci, B.; Cossi, M.; Scalmani, G.; Rega, N.; Petersson, G. A.; Nakatsuji, H.; Hada, M.; Ehara, M.; Toyota, K.; Fukuda, R.; Hasegawa, J.; Ishida, M.; Nakajima, T.; Honda, Y.; Kitao, O.; Nakai, H.; Klene, M.; Li, X.; Knox, J. E.; Hratchian, H. P.; Cross, J. B.; Bakken, V.; Adamo, C.; Jaramillo, J.; Gomperts, R.; Stratmann, R. E.; Yazyev, O.; Austin, A. J.; Cammi, R.; Pomelli, C.; Ochterski, J. W.; Ayala, P. Y.; Morokuma, K.; Voth, G. A.; Salvador, P.; Dannenberg, J. J.; Zakrzewski, V. G.; Dapprich, S.; Daniels, A. D.; Strain, M. C.; Farkas, O.; Malick, D. K.; Rabuck, A. D.; Raghavachari, K.; Foresman, J. B.; Ortiz, J. V.; Cui, Q.; Baboul, A. G.; Clifford, S.; Cioslowski, J.; Stefanov, B. B.; Liu, G.; Liashenko, A.; Piskorz, P.; Komaromi, I.; Martin, R. L.; Fox, D. J.; Keith, T.; Al-Laham, M. A.; Peng, C. Y.; Nanayakkara, A.; Challacombe, M.; Gill, P. M. W.; Johnson, B.; Chen, W.; Wong, M. W.; Gonzalez, C.; Pople, J. A. *Gaussian 03*; Gaussian, Inc.: Pittsburgh, PA, 2003.

monochromator coupled to a photoelectron multiplier tube, and a digital oscilloscope. The entire setup was controlled from a personal computer using LabView software. In order to avoid depletion of the precursor and product build-up, a flow cell was used. Toluene solutions containing 13.2 μmol/L C_{60} and 1 mmol/L **4a** were used for the LFP experiments.

DFT Calculations. Calculations were performed with the Gaussian 03 program package.[25] Geometries and frequencies were calculated at the B3LYP/6-31G(d) level of theory and scaled with a factor of 0.9614[26] for better comparison with the experiment.

Monte Carlo Integration. The Monte Carlo integration of the mechanism was accomplished according to the algorithm described by Schaad.[27] A program written using Visual Basic 6.0 was used for the evaluation of data (the program is available from the authors on request). A 300 × 300 grid was used, and the cells of the grid were filled at 80% with the reactants $^1O_2$ and **4a** to avoid overflow of the grid during the simulation. The number of molecules used during the simulation was greater than 10^4, thus limiting the error of the simulation to ~1%.[27]

For the simulation of the step scan FTIR experiments we assumed that the initial concentration of $^1O_2$ equals the initial concentration of C_{60} (0.26 mmol/L) and the initial concentration of **4a** was 2 mmol/L (Table 1). The following equations have been used to map the Monte Carlo simulation into the chemical system:

$$-\frac{\mathrm{d}c(\mathbf{4a})}{\mathrm{d}t} = k_1 c(\mathbf{4a}) c(^1O_2) \tag{1}$$

$$-\frac{\mathrm{d}[\mathbf{4a}]}{\mathrm{d}m} = n_1 p[\mathbf{4a}][^1O_2] \tag{2}$$

$$\frac{\mathrm{d}c(\mathbf{1a})}{\mathrm{d}t} = k_2 c(\mathbf{5a}) \tag{3}$$

$$\frac{\mathrm{d}[\mathbf{1a}]}{\mathrm{d}m} = n_2 p[\mathbf{5a}] \tag{4}$$

$$\frac{\mathrm{d}c(\mathbf{7a})}{dt} = k_3 c(\mathbf{5a}) \tag{5}$$

$$\frac{\mathrm{d}[\mathbf{7a}]}{\mathrm{d}m} = n_3 p[\mathbf{5a}] \tag{6}$$

Where [**x**], c(**x**) represent the stochastic (fraction of molecules in the grid) and real concentration respectively, and m and t the "stochastic" and real time. The scaling coefficients are indicated as α ([x] = αc(**x**)) and β ($m = \beta t$). The variable p is the grid probability (e.g., a grid containing n rows and n columns will have for every cell a constant probability $p = 1/n^2$).

Dividing eq 1 by eq 2 results in

$$\frac{\frac{\mathrm{d}c(\mathbf{4a})}{\mathrm{d}t}}{\frac{\mathrm{d}[\mathbf{4a}]}{\mathrm{d}m}} = \frac{k_1 c(\mathbf{4a}) c(^1O_2)}{n_1 p[\mathbf{4a}][^1O_2]} \tag{7}$$

$$\frac{\beta}{\alpha} = \frac{k_1}{n_1 p \alpha^2} \tag{8}$$

From eq 8 we obtain for k_1

$$k_1 = n_1 p \alpha \beta \tag{9}$$

Using the same procedure, eqs 10 and 11 are obtained for k_2 and k_3.

$$k_2 = n_2 p \beta \tag{10}$$

$$k_3 = n_3 p \beta \tag{11}$$

The values found for α and β were 360 L mol^{-1} and 6.875 × 10^7 cycles/s, respectively, and $p = 1/(9 \times 10^4)$, using the values $n_1 = 280$, $n_2 = 1023$, $n_3 = 750$. The values for the rate constants are then $k_1 = 7.7 \times 10^7$ L mol^{-1} s^{-1}, $k_2 = 7.81 \times 10^5$ s^{-1}, $k_3 = 5.73 \times 10^5$ s^{-1}.

Simulation of Time-Resolved IR Spectra. Time-resolved IR spectra were simulated by "mixing" the Monte Carlo and DFT calculations.

The mapping was carried out using the following equation:

$$\sum_i \Delta C_t^{\mathrm{MMC}}(i) \times S_i^{\mathrm{DFT}} \tag{12}$$

where the sum runs over the species involved in the mechanism. The factor $\Delta C_t^{\mathrm{MMC}}(i)$ in the sum is the concentration (after mapping Monte Carlo into the chemical system) of the component i at time t minus the concentration of the component i at the initial time. The superindex MMC stands for Mapped Monte Carlo. The factor S_i^{DFT}inside the sum is the scaled calculated spectrum of component i.

Acknowledgment. J.T. is indebted to Dr. Christoph Kolano and Dr. Goetz Bucher for their introduction to step-scan and LFP, respectively. This work was financially supported by the Deutsche Forschungsgemeinschaft and the Fonds der Chemischen Industrie.

Supporting Information Available: Time resolved IR spectra recorded in toluene (S1); transient traces at 2041 and 2219 cm^{-1} corresponding to the experiment in toluene (S2); Cartesian coordinates and total energies of **1a**, **4a**, **5a**, **7a**, and N_2O (S4−S8); set-up for step-scan time-resolved FTIR measurements (S9); and transient traces recorded at 500 nm in toluene containing C_{60} in the presence and absence of oxygen (S10). This material is available free of charge via the Internet at http://pubs.acs.org.

JO800955W

(26) Scott, A. P.; Radom, L. *J. Phys. Chem.* **1996**, *100*, 16502–16513.
(27) Schaad, L. J. *J. Am. Chem. Soc.* **1963**, *85*, 3588–3592.